

3-1-2007

Abundance Analysis of the Extremely Fast ONeMg Novae V838 Herculis and V4160 Sagittarii

G.J. Schwarz

S.N. Shore

S. Starrfield

K.M. Vanlandingham
kvanlandingham@wcupa.edu

Follow this and additional works at: http://digitalcommons.wcupa.edu/geol_facpub



Part of the [Astrophysics and Astronomy Commons](#)

Recommended Citation

Schwarz, G. J., Shore, S. N., Starrfield, S., & Vanlandingham, K. M. (2007). Abundance Analysis of the Extremely Fast ONeMg Novae V838 Herculis and V4160 Sagittarii. *Astrophysical Journal*, 657(1), 453-464. <http://dx.doi.org/10.1086/510661>

This Article is brought to you for free and open access by the Geology & Astronomy at Digital Commons @ West Chester University. It has been accepted for inclusion in Geology & Astronomy Faculty Publications by an authorized administrator of Digital Commons @ West Chester University. For more information, please contact wccressler@wcupa.edu.

ABUNDANCE ANALYSIS OF THE EXTREMELY FAST ONeMg NOVAE V838 HERCULIS AND V4160 SAGITTARI

GREG J. SCHWARZ

Department of Geology and Astronomy, West Chester University, West Chester, PA; gschwarz@as.arizona.edu

STEVEN N. SHORE

Dipartimento di Fisica “Enrico Fermi,” Università di Pisa, I-56127 Pisa, Italy; INFN-Sezione di Pisa; shore@df.unipi.it

SUMNER STARRFIELD

School of Earth and Space Exploration, Arizona State University, Tempe, AZ; sumner.starrfield@asu.edu

AND

KAREN M. VANLANDINGHAM

Department of Geology and Astronomy, West Chester University, West Chester, PA; kvanlandingham@wcupa.edu

Received 2006 April 26; accepted 2006 November 6

ABSTRACT

V838 Her and V4160 Sgr were two of the fastest classical novae ever observed, exhibiting light curve declines of 2 mag in less than 2 days. Both novae also showed strong neon emission lines, indicative of an outburst occurring on an oxygen-neon-magnesium white dwarf. Being the brighter of the two, V838 Her has an extensive set of X-ray to radio observations obtained during its first year after outburst. V4160 Sgr has a more modest set of ultraviolet and optical spectra, which show it to be similar to V838 Her, not just in its light curve evolution but also in its spectral development. The observed attributes imply that these novae occurred on extremely massive white dwarfs. This paper uses the Cloudy photoionization code to fit multiple epochs of emission line spectra to determine the elemental abundances of the ejecta of V838 Her and V4160 Sgr.

Subject headings: stars: abundances — stars: individual (V838 Herculis, V4160 Sagittarii) — novae, cataclysmic variables

1. INTRODUCTION

The year 1991 was a banner year for classical novae, with an unusual number of bright and interesting novae discovered. Many of these novae were observed frequently during their evolution, and with instruments across the electromagnetic spectrum. The two fastest novae, as measured by the decay of their visual light curves, were V838 Her and V4160 Sgr. These novae developed strong neon lines during their nebular phases, implying that the explosions occurred on the surface of an oxygen-neon-magnesium (ONeMg) white dwarf (WD). The speed at which they initially faded also implies that the explosions occurred on fairly massive WDs. One purpose of this paper is to demonstrate that the ejected gases are enriched in neon and that the outburst did occur on ONeMg WDs.

Much is known about V838 Her thanks to extensive multi-wavelength observations and analyses (see Vanlandingham et al. 1996, and references within). Briefly, V838 Her reached a visual maximum of 5th magnitude on 1991 March 25 and within 2 days had declined by 2 mag making it one of the fastest novae ever observed (see Fig. 1). Optical spectra obtained after maximum light showed wide, flat-topped emission lines, indicating a high expansion velocity. The FWZI of $H\alpha$ was 7000 km s^{-1} 1 day after maximum (Harrison et al. 1991). An increase in the infrared beginning 5 days after maximum marked the beginning of dust formation, which peaked 20 days later (Woodward et al. 1992). The amount of dust formed was small, as evidenced by the fact that the infrared luminosity was only $\sim 3\%$ – 5% of the total luminosity (Woodward et al. 1992; Lynch et al. 1992). V838 Her was also detected by *Röntgensatellit* (ROSAT) 5 days after outburst (Lloyd et al. 1992). The X-rays were thought to have originated in a hot, shock-heated gas, although the resolution of

the PSPC detector on ROSAT is insufficient to confirm this assumption. Subsequent ROSAT observations 1 and 1.5 yr after discovery yielded a faint X-ray source whose luminosity was of order 10^{32} – $10^{33} \text{ ergs s}^{-1}$ (O’Brien et al. 1994; Szkody & Hoard 1994). This luminosity is many orders of magnitude lower than expected from hydrogen burning on a WD and indicated that nuclear burning had ceased in V838 Her less than 1 yr after outburst.

One of the lesser known fast novae of 1991 was V4160 Sgr. It was discovered on 1991 July 29 (Bateson et al. 1991) at 7th magnitude, when it was already on the decline. Because it was fainter at discovery and perhaps due to observer exhaustion from the numerous novae found in 1991, V4160 Sgr was not observed nearly as extensively as V838 Her. There was no reported infrared photometry in the literature to determine whether V4160 Sgr formed dust. Likewise, the lack of X-ray observations meant that there were no constraints on its nuclear burning timescale. However, the optical (della Valle & Prins 1991; Kingsburgh et al. 1991; Dopita et al. 1991; Williams et al. 1994) and UV observations that do exist show some amazing similarities to V838 Her. The light curve of V4160 Sgr (also in Fig. 1) showed that this nova also declined 2 mag within 2 days after discovery. With the exception of broader emission lines, the early optical spectra of V4160 Sgr were identical to those of V838 Her (Williams et al. 1994). With an $H\alpha$ FWZI of 9500 km s^{-1} recorded 3 days after discovery (della Valle & Prins 1991), V4160 Sgr exhibits one of the largest expansion velocities ever measured in a classical nova.

The optical and UV spectral development of these two novae were extremely similar. Both displayed strong optical [Ne III] and [Ne V] lines only a few weeks after outburst. After declining about 8 mag in 1 month, both novae entered the nebular phase. Figure 2 shows the UV and optical spectra of V838 Her (scaled by 0.25) and V4160 Sgr approximately 1 month after maximum.

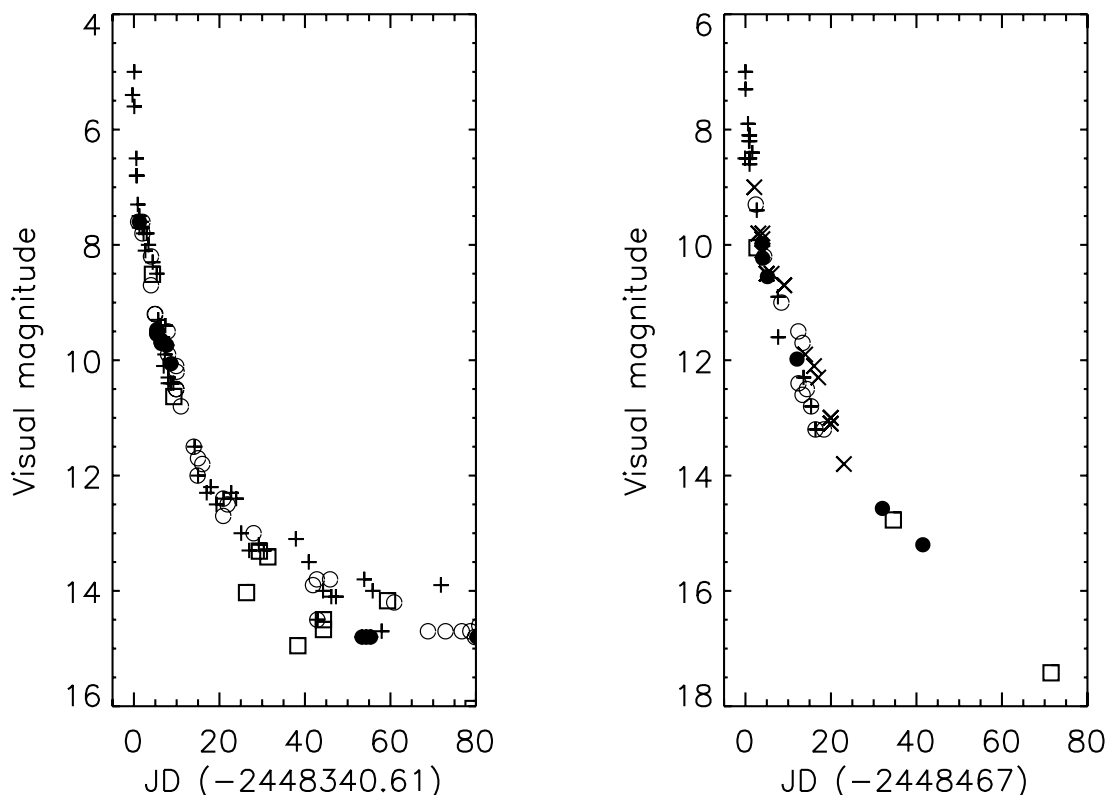


FIG. 1.—Visual light curves of V838 Her (*left*) and V4160 Sgr (*right*) available in the IAU circulars, and AFOEV and VSOLJ databases. The pluses are visual estimates, the filled circles are V -band magnitudes, the open circles are AFOEV V -band magnitudes, and the crosses mark VSOLJ visual estimates. The squares are V -band magnitude derived from the spectroscopy.

The continuum shapes are the same, and many of the emission lines have similar strengths. The main differences are that V838 Her appears to show stronger carbon and sulfur lines, while V4160 Sgr has stronger nitrogen and oxygen lines.

Given the similarities between the two novae, an abundance analysis and comparison can provide insights on outbursts occurring on massive ONeMg WDs. This paper presents an elemental abundance analysis of V4160 Sgr and a reanalysis of V838 Her. The V838 Her analysis builds on the data and results in Vanlandingham et al. (1996, 1997) by incorporating additional observations and modeling multiple dates to constrain the model parameters. The

final V838 Her solution is used as a template to initially estimate the V4160 Sgr abundance solution. Section 2 describes the data used in the analysis. In § 3 the photoionization model techniques are described. Section 4 discusses the results of the model fits to the observed data for V838 Her and V4160 Sgr. A review of all the ONeMg novae recently modeled with similar techniques is provided in § 5. The review covers many ONeMg novae over a wide range of speed classes, which is useful for detecting predicted trends and determining ONeMg novae contributions to the ISM and presolar grains in meteorites.

2. THE EMISSION LINE SPECTRA

The new analysis of V838 Her included two supplemental dates with nearly simultaneous optical and UV observations, in addition to the single date assessed by Vanlandingham et al. (1996). For the date common to both analyses, 1991 May 24, we have included more emission lines (18 vs. 30 lines). With this larger data set, a global model must be able to fit a wider range of evolving ionization lines. In essence, the more lines to fit the more constrained the final solution becomes. All the observations used come from Vanlandingham et al. (1996) and Williams et al. (1994). The dates span the time from 28 to 79 days after outburst, where day zero is taken as 1991 March 25. Finally, a fourth date from Williams et al. (1994) taken 148 days after maximum, was also included as another check on the model parameters derived from the previous three date solutions. By this time V838 Her was too faint to be observed by *IUE*, so the model only includes optical lines, but the line list is supplemented by the addition of the [S II] (9069, 9532 Å) line ratios obtained at the same time by Matheson et al. (1993).

Williams et al. (1994) obtained optical spectra of V4160 Sgr on 1991 August 1.22, September 2.08, and October 9.04. The

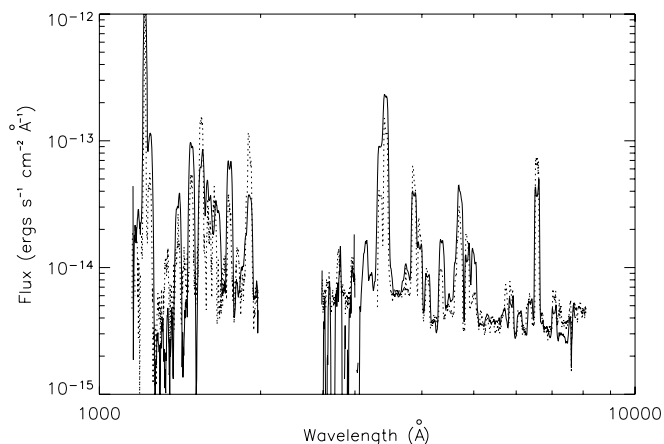


FIG. 2.—Ultraviolet and optical spectra of V4160 Sgr (*solid line*) and V838 Her (*dotted line*) obtained 34 and 28 days after maximum, respectively. None of the spectra have been corrected for reddening. The V838 Her data have been scaled by 0.25, which is equivalent to a magnitude difference of 1.5.

nova was observed on five separate occasions with *IUE* on 1991 August 20, 26, and 30 and September 2 and 12. With this limited data set there is only one date with simultaneous optical and UV observations. This date, 1991 September 2, occurred 35 days after visual maximum, where 1991 July 29 is taken as day zero. The September 12 *IUE* and the October 9 Williams et al. (1994) spectra are also separately used in the analysis as additional constraints on the V4160 Sgr model.

When combining UV and optical data, the absolute calibration between the two wavelength regions is required. In order to confirm that the absolute optical flux calibration was correct, a *V*-band magnitude was calculated for each optical spectrum since there might be light losses at the spectrographic slit. These magnitudes are shown in Figure 1 as open squares. The optical spectra obtained when the novae were bright agreed with the reported visual and *V*-band magnitudes. All spectra that did not agree with the observed light curves were scaled until their *V*-band magnitudes agreed with the observed values. The V838 Her spectra were scaled to agree with the photometry of Ingram et al. (1992). The May 24 and June 12 optical spectra, which are used in the model analysis, require scaling factors of 0.5 and 2.5, respectively, to fit the observed light curve.

Also of critical importance to deriving an accurate abundance solution is a well-determined reddening value for the nova. A value of $E(B - V) = 0.6$ for V838 Her is taken from Vanlandingham et al. (1996) and Matheson et al. (1993). For V4160 Sgr, Mason et al. (2002) derives $A_V = 1.09 \pm 0.13$ from the Na I equivalent width measurement. This value is consistent with $E(B - V) = 0.37$ given by the Schlegel et al. (1998) extinction maps. However, these values likely underestimate the true reddening. V4160 Sgr is located in the Galactic plane, where the accuracy of the Schlegel et al. (1998) extinction maps decreases greatly since contaminating sources at $|b| < 5^\circ$ have not been removed. The Na I measurement was from a single early observation that the authors state is likely contaminated by the nearby He I emission line. Without additional equivalent width data, the derived extinction from the Na I equivalent width must be treated as a lower limit. Another method of determining the reddening toward V4160 Sgr follows from the work in Shore et al. (2003). They showed that the intrinsic spectra of 3 ONeMg novae (V382 Vel, V1974 Cyg, and LMC 2000) were similar when scaled by their t_2 decline times. The reason for the similarities is that early in the outburst the spectral energy distribution is primarily determined by the decline rate of the nova shell opacity, which in turn is a function of the amount of mass ejected and the expansion velocity. Given that V838 Her and V4160 Sgr are both ONeMg novae with the same decay times, a reasonable assumption is that early spectra, obtained at approximately the same time after outburst, should be similar. Figure 2 shows that at approximately 1 month after each outburst the $\sim 10^3$ – 10^4 Å energy distributions of the two novae were essentially identical. The similarities imply that the reddening determined for V838 Her can also be applied to V4160 Sgr, so that their spectral developments remain parallel. Therefore, given the caveats in the other methods, the V838 Her reddening is adopted for V4160 Sgr.

The dereddened emission line fluxes relative to H β are given in Table 1. Hereafter, each modeled date is referenced by the number of days since maximum and prefaced with a “D,” e.g., D60 is May 24 for V838 Her. The line fluxes were measured by integrating individual lines.¹ The strongest line ratios, with values ≥ 1 , have an estimated uncertainty of 25%, which includes contributions from relative spectral calibration and the estimate

of the continuum level. For weak lines the difficulties in determining the continuum level increase the uncertainty to 50%. In cases where strong lines were present, but severely blended with neighboring lines due to the extreme expansion velocities, the uncertainty level is also 50%. This is a greater problem in the UV between 1550 and 1667 Å and particularly in V4160 Sgr, whose expansion velocity exceeded that of V838 Her.

3. PHOTOIONIZATION MODEL ANALYSES

The Cloudy 94.00 photoionization code (Ferland et al. 1998, and references therein) is used to model the physics of the novae ejecta. The major attributes of each Cloudy model that determine the output are the ejected shell and the illuminating source parameters. The source parameters are the luminosity and spectral energy distribution. The shell parameters include the shape, the hydrogen density, the density structure, the elemental abundances relative to hydrogen, and the covering factor. The covering factor is the fraction of 4π sr enclosed by the model shell (see Schwarz 2002; Vanlandingham et al. 2005 for full details).

The ejecta are assumed to be spherical shells with inner and outer radii defined by the expansion velocities. The hydrogen density structure varies as r^{-3} to provide a constant mass per unit volume throughout the model shell. The ratio of the filled to vacuum volumes in the ejecta are set to 0.2, which is the value used in other recent Cloudy studies (Schwarz 2002; Vanlandingham et al. 2005). To minimize the number of free parameters, the density power, filling factor, and inner and outer radii are held constant during the iterative process of fitting the observations. The hydrogen density, underlying luminosity, and effective blackbody temperature are allowed to vary.² In addition, only the abundances of elements with observed lines are allowed to vary. All others are fixed at their solar values. The goodness of fit is estimated from the χ^2 of the model.

A successful model must be consistent with the results from other dates in addition to having a low χ^2 value (typically, a reduced χ^2 of 1–2). The final elemental abundances of the novae are the mean values from each epoch’s best-fit model, excluding dates when no lines of a particular element were observed. The corresponding uncertainties are the standard deviation of the mean from each epoch.

3.1. Multicomponent Modeling

Images of old novae show extremely complex structure. The presence of multi-peaked components and broad wings in emission lines is an indication of slower moving clumps embedded in a diffuse gas (see images of V1974 Cyg and T Pyx; Paresce 1994; Paresce et al. 1995; Shara et al. 1997). Clumps and density gradients can make modeling difficult, particularly when the emission arises in both a wind and an ejected shell. The emission contributions from each of the different components depends on the particulars of the nova outburst and when the observations are obtained (Williams 1992). Observations obtained when the spectra are transitioning from the optically thick to nebular phases can be especially hard to fit, particularly if a nova wind is active.

In past photoionization analyses this difficulty could be ignored if the available observations: (1) only sampled a small range of ionization states, or (2) were obtained much later in the outburst when the nebular shell contribution dominated the spectrum. An example is the moderately fast ONeMg nova QU Vul (Schwarz

¹ See Schwarz (2002) for a review of the techniques used to estimate individual components for different line blends.

² We emphasize that our goal is to determine the elemental abundances of the ejecta and those are relatively insensitive to the shape of the incident source spectral energy distribution. More important is that the underlying source produce enough ionizing photons (see Schwarz 2002; Vanlandingham et al. 2005).

TABLE 1
OBSERVED AND BEST-FIT CLOUDY MODEL LINE FLUXES RELATIVE TO H β

Line	λ	Obs	C94	χ^2	Obs	C94	χ^2	Obs	C94	χ^2	Obs	C94	χ^2
V838 Her													
		APRIL 22 (D28)			MAY 24 (D60)			JUNE 12 (D79)			AUGUST 20 (D148)		
N v	1240	25.1	27.12	0.10	4.4	5.68	0.34	4.3	4.33	0.00
C II	1335	3.2	0.80	9.00
Blend	1400	4.2	5.84	2.44
Si IV ^a	1397	...	2.85
O IV ^a	1402	...	1.85
S IV ^a	1406	...	1.14
N IV	1486	10.1	11.43	0.30	2.6	2.51	0.00	2.5	2.91	0.11
C IV	1549	39.5	60.05	4.33	10.8	11.22	0.02	12.3	13.19	0.08
[Ne IV]	1602	5.2	2.97	2.94	3.8	4.98	0.39	4.3	4.93	0.09
He II	1640	6.9	6.82	0.00	2.6	4.38	1.88	4.6	5.70	0.23
N III	1750	6.7	5.77	0.31	3.0	1.18	1.47	2.2	1.07	1.06
Blend	1810	1.7	1.03	0.62
Si II ^a	1808	...	0.45
[Ne III] ^a	1815	...	0.58
Si III	1888	4.0	3.52	0.23	2.0	1.23	0.59	2.2	2.37	0.10
C III	1909	29.4	20.89	1.34	10.8	6.12	3.00	11.6	4.38	6.19
Blend	2330	7.3	1.99	8.47	3.4	0.40	3.11
[O III] ^a	2321	...	0.07	0.04
C II ^a	2326	...	1.37	0.20
Si II ^a	2335	...	0.55	0.16
[Ne IV]	2424	1.2	0.78	0.49
Al II	2665	0.4	0.33	0.43	0.2	0.19	0.02
Mg II	2798	1.2	1.47	0.78	0.4	0.29	0.32
[Ne V]	2976	0.71	0.65	0.09	0.4	0.22	0.81
He II	3203	0.5	0.41	0.11
[Ne V]	3346	2.7	3.13	0.40	17.3	7.83	4.79	18.9	10.61	3.08	39.2	32.96	0.41
[Ne V]	3426	13.2	8.56	1.98	33.3	21.44	2.03	47.8	29.04	2.46	94.6	90.25	0.03
[S III]	3722	0.5	0.25	0.94	0.7	0.32	1.11
[Ne III] ^b	3869	4.0	6.02	4.08	21.7	14.73	1.65	27.6	18.06	1.91	41.0	37.71	0.10
[Ne III] ^b	3968	1.3	1.81	3.26	5.8	4.44	0.88	7.9	5.44	1.55	10.9	11.36	0.03
Blend	4100	0.5	0.42	0.1	0.8	0.43	3.42	1.1	0.56	0.96	2.4	1.64	1.60
S II ^a	4074	...	0.07	0.13	0.28	1.37	...
H δ ^a	4100	...	0.35	0.30	0.28	0.27	...
Blend	4350	0.5	0.56	0.24	0.6	0.70	0.44	0.6	0.72	0.16	0.8	0.70	0.25
H γ ^a	4340	...	0.56	0.51	0.49	0.48	...
[O III] ^a	4363	0.19	0.23	0.22	...
Blend	4700	2.0	1.54	0.85	3.0	1.75	2.77	3.1	1.92	2.30	3.4	2.75	0.58
He II ^a	4686	...	0.86	0.60	0.78	1.16	...
Ne IV ^b	4720	...	0.68	1.15	1.14	1.59	...
H β	4861	1.0	1.00	0.00	1.0	1.00	0.00	1.0	1.00	0.00	1.0	1.00	0.00
[O III] ^b	4959	0.1	0.08	0.02	0.2	0.17	0.08	0.5	0.42	0.09
[O III] ^b	5007	0.2	0.22	0.00	0.5	0.37	0.13	0.6	0.50	0.12	1.3	1.20	0.19
He II	5412	0.1	0.07	1.22	0.1	0.05	0.10	0.1	0.07	0.13	0.1	0.09	0.31
Blend	5740	0.2	0.10	1.00	0.5	0.10	2.50	0.7	0.15	2.50	0.8	0.75	0.06
[Fe VII] ^a	5722	...	0.06	0.07	0.08	0.09	...
[N II] ^a	5755	...	0.04	0.03	0.07	0.66	...
He I	5876	0.2	0.20	0.01	0.1	0.10	0.01	0.2	0.14	0.11
[Fe VII]	6087	0.1	0.09	0.29	0.1	0.10	0.00	0.1	0.12	0.01	0.2	0.14	0.02
[S III]	6312	0.2	0.18	0.10	0.3	0.42	0.29	0.6	0.54	0.04	1.0	1.10	0.16
Blend	6565	3.4	4.37	1.30	2.0	3.20	1.49	2.8	2.90	0.02	5.5	4.26	0.81
[N II] ^{a,b}	6548	0.37	...
H α ^a	6563	...	4.37	3.22	2.88	2.79	...
[N II] ^{a,b}	6584	0.02	1.10	...
He I	7065	0.1	0.16	0.24	0.1	0.07	0.02	0.1	0.10	0.00	0.1	0.05	0.82
[S III]	9069	0.3	0.29	0.10	2.0 ^d	1.95	0.01
[S III]	9532	0.1 ^c	0.11	0.15	0.7	0.71	0.02	5.0 ^d	4.84	0.02

TABLE 1—Continued

Line	λ	Obs	C94	χ^2	Obs	C94	χ^2	Obs	C94	χ^2
V4160 Sgr										
SEPTEMBER 2 (D35)			SEPTEMBER 12 (D45) ^c				OCTOBER 9 (D72)			
N v	1240	74.3	58.66	1.11	2.7	2.46	0.26
C II	1335	0.1	0.03	1.81
Blend	1400	12.7	10.64	0.42	0.4	0.31	0.31
Si IV ^a	1397	...	5.13	0.09
O IV] ^a	1402	...	5.51	0.22
N IV]	1486	33.7	33.28	0.00	1.0	1.00	0.00
C IV]	1549	27.8	22.63	0.86	0.9	0.58	0.56
Blend	1590	16.9	3.88	2.37	0.8	0.31	1.52
[Ne v] ^a	1575	...	1.63	0.09
[Ne IV] ^a	1602	...	2.25	0.22
He II	1640	8.3	7.24	0.41	0.2	0.25	0.05
O III]	1666	5.6	5.54	0.00	0.2	0.14	0.39
N III]	1750	23.4	21.53	0.16	0.5	0.41	0.60
Si III]	1888	6.8	7.65	0.39	0.1	0.13	0.13
C III]	1909	9.7	9.81	0.00	0.2	0.22	0.17
Mg II	2798	0.4	0.41	0.10
[Ne v]	2976	0.1	0.03	2.35
[Ne v]	3346	10.7	11.01	0.02	20.5	19.52	0.06
[Ne v]	3426	35.5	30.15	0.57	67.4	53.46	1.07
[Ne III] ^b	3869	4.6	3.50	1.44	18.3	19.4	0.09
[Ne III] ^b	3968	1.4	1.05	1.53	5.8	5.85	0.00
Blend	4350	1.5	1.47	0.01	2.3	2.35	0.01
H γ ^a	4340	...	0.51	0.48	...
[O III] ^a	4363	...	0.96	1.87	...
Blend	4700	2.5	1.47	2.75	3.9	3.10	0.67
He II ^a	4686	...	0.95	1.52	...
Ne IV] ^a	4720	...	0.52	1.58	...
H β	4861	1.0	1.00	0.00	1.0	1.00	0.00
[O III] ^b	4959	0.2	0.22	0.02	3.0	3.18	0.09
[O III] ^b	5007	0.6	0.65	0.00	9.0	9.17	0.01
[N II]	5755	0.6	0.38	0.42
He I	5876	0.2	0.13	0.12	0.2	0.12	0.71
[Fe VII]	6087	0.1	0.09	0.01	0.3	0.32	0.01
Blend	6350	0.2	0.25	0.60	0.1	0.09	0.00
[O I] ^a	6300	...	0.12	0.07	...
[O I] ^a	6363	...	0.04	0.02	...
[Fe X] ^a	6375	...	0.09
Blend	6565	2.7	3.22	1.3	2.2	2.88	1.52
[N II] ^{a,b}	6548	...	0.03	0.03	...
H α ^a	6563	...	3.10	2.75	...
[N II] ^{a,b}	6584	...	0.09	0.10	...
He I	7065	0.1	0.09	0.08	0.1	0.07	0.52
[O II] 7325	0.2	0.28	1.3

NOTE.—Dereddened with $E(B - V) = 0.6$.

^a The χ^2 of the blended line above is calculated with the summed contribution of the C94 lines.

^b Deblended assuming the low-density limit, where the line ratios are proportional to the line statistical weights.

^c From Williams et al. (1994) 1991 April 25 spectrum.

^d From Matheson et al. (1993).

^e Relative to N IV] (1486 Å).

2002), which although it had a tremendous amount of multiwavelength data available, was well modeled by a single Cloudy component during the nebular phase. During the nebular phase, the clumps in QU Vul had become progressively more ionized and contributed less to the emerging spectrum. However, in both V838 Her and V4160 Sgr the best multiwavelength data were obtained during the transition to the nebular stage, and thus show simultaneous emission from both low- and high-ionization lines. For example, both novae have large [Ne v] (3346, 3426 Å) to [Ne III] (3869, 3968 Å) ratios that cannot be fit with a single Cloudy model. This presents a serious problem for a one com-

ponent model since these neon lines are some of the strongest in the spectra.

To address this problem each date is fit with the sum of two distinct models (see also Hayward et al. 1996; Vanlandingham et al. 2005) to incorporate the contributions of clumping and density gradients into the final model. The first component has a high density to fit the lower ionization lines. This (clump) portion fits the majority of the observed lines, but systematically under-represents the highest ionization lines. A second (diffuse) model with a lower density is used to make up the difference in the high-ionization lines while not upsetting the clump contribution to the

TABLE 2
V838 HER BEST-FIT CLOUDY MODEL PARAMETER

Parameter	April 22 (D28)	May 24 (D60)	June 12 (D79)	August 20 (D148)
T_{BB} ($\times 10^5$ K) ^a	3.2	2.0	2.5	4.0
Source luminosity ($\times 10^{37}$ ergs s ⁻¹) ^a	10	7.9	3.4	1.0
Diffuse hydrogen density ($\times 10^7$ cm ⁻³) ^a	12.6	1.26	0.63	0.10
Clump hydrogen density ($\times 10^7$ cm ⁻³) ^a	37.8	3.8	1.9	0.30
Inner radius ($\times 10^{15}$ cm) ^b	0.77	1.55	2.09	3.90
Outer radius ($\times 10^{15}$ cm) ^b	1.29	2.57	3.47	6.46
Clump to diffuse covering factor ratio ^a	50/50	30/70	40/60	25/75
He/He _⊙ ^{a,c}	1.5 (6)	1.1 (5)	1.6 (5)	1.5 (2)
C/C _⊙ ^{a,c}	7.2 (4)	9.1 (3)	5.8 (2)	9.1 (0)
N/N _⊙ ^{a,c}	31.0 (4)	33.1 (4)	33.1 (5)	61.7 (3)
O/O _⊙ ^{a,c}	3.2 (4)	1.6 (3)	1.6 (3)	1.0 (3)
Ne/Ne _⊙ ^{a,c}	50.1 (8)	50.1 (8)	50.1 (6)	63.1 (5)
Mg/Mg _⊙ ^{a,c}	0.6 (1)	2.2 (1)	1.1 (0)	1.1 (0)
Al/Al _⊙ ^{a,c}	7.9 (1)	50.1 (1)	1.3 (0)	1.3 (0)
Si/Si _⊙ ^{a,c}	4.4 (4)	11.0 (2)	11.0 (1)	1.1 (0)
S/S _⊙ ^{a,c}	29.5 (4)	46.8 (3)	29.5 (5)	29.5 (4)
Fe/Fe _⊙ ^{a,c}	2.9 (2)	1.1 (2)	1.1 (2)	0.9 (2)
Ejected mass ($\times 10^{-4}$ M _⊙)	1.2	0.8	1.1	0.94
Lines used	33	29	27	17
dof ^d	19	14	14	6
Total χ^2	37.6	34.0	24.4	5.5

^a Free parameter in the optimization. All models had a hydrogen power laws of -3 , filling factors of 0.2, and filling factor laws of 0.

^b Calculated assuming an inner and outer expansion velocity of 3000 and 5000 km s⁻¹, respectively. Not a free parameter in the models.

^c Where log(solar number abundances relative to hydrogen) He: -1.0 , C: -3.61 , N: -4.22 , O: -3.34 , Ne: -3.93 , Mg: -4.47 , Al: -5.63 , Si: -4.49 , S: -4.86 , and Fe: -4.55 (where all abundances are taken from Asplund et al. [2005] except for H and Ne, which are from Grevesse & Noels [1993]). The number in the parentheses indicates the number of Cloudy lines used in the analysis.

^d Equal to the number of observed lines used in the analysis minus the number of free parameters in the model.

spectrum. The majority of the model parameters are the same in both models in order to reduce the number of free parameters in the final combined model. This simplification means that each component is subjected to the same ionization source and has the same basic shell structure including abundances. The only parameters that are unique to each component are the hydrogen densities at the inner radius and the covering factors, plus an added stipulation that the sum of the two covering factors be less than or equal to 1. Thus, with the addition of a second component, the overall number of free parameters only increases by 2: the second components initial density and covering factor. The final model line ratios are the sum of each component's line ratio multiplied by its covering factor, since the covering factor scales with the Cloudy line luminosities.

This method does not treat clumps realistically as individual blobs embedded in the diffuse gas. In terms of individual photons, $X\%$ travel through regions of the ejected shell that are clump dominated, while the remaining $(100-X)\%$ photons only interact with the diffuse region. Thus, the method is only a first-order approximation to incorporating density gradients into the photoionization analysis. There is no coupling or interaction between the two, as expected in a true two-dimensional model, where shielding by embedded density inhomogeneities would be considered in the radiation transport calculations (Williams 1992). However, this two-component model is a reasonable approximation and has worked for V1974 Cyg (Vanlandingham et al. 2005) and V382 Vel (Shore et al. 2003).

4. MODEL RESULTS

4.1. The V838 Her Model Fits to the D29, D60, D80, and D149 Data

For V838 Her, the inner and outer radii were constrained for each model by assuming a minimum and maximum expansion

velocity of 3000 and 5000 km s⁻¹, respectively, multiplied by the number of days past outburst. The best-fit two-component model parameters are given in Table 2. The reduced χ^2 for the four dates range from 0.9 to 2.4. The predicted line ratios and corresponding χ^2 values for the observed lines for each model are provided in Table 1. Overall, the fits are very good, with the largest χ^2 values coming from the fits to the strong carbon and neon lines. The general problem is that the Cloudy models predict more flux for certain ionization states (e.g., C iv 1550 Å) and less for others of the same elements (e.g., C iii] 1909 Å). On the first model date, D28, the worst fit, carbon and neon lines contribute over 60% to the χ^2 , but this fit does minimize the χ^2 contributions of the discrepant lines. The problem is not as severe on D60 and D79, and the problem disappears on D148, where there is no UV data.

The ratio of the clump to diffuse hydrogen density was 3 in all models. These values are consistent with those found in a similar two-component analysis of V1974 Cyg (Vanlandingham et al. 2005). The clump to diffuse covering factor ratio was ≤ 1 , indicating that the ejecta volume was generally dominated more by the diffuse gas; however, given the density difference, it was the clumps that dominate the ejected mass.

On the first date, the model luminosity was 10^{38} ergs s⁻¹, but it declined by a factor of 10 within the next 4 months. The luminosity on D60 is more than a factor of 10 larger than found by Vanlandingham et al. (1996), but the rapid decline in these models is consistent with the lack of an X-ray detection 1 yr after outburst (O'Brien et al. 1994). It is also consistent with the theory that outbursts on massive WDs leave less material behind to power stable hydrogen burning than on less massive WDs (Starrfield et al. 1991).

The final abundances are compared to those derived by Vanlandingham et al. (1996, 1997) in Table 3. There is good agreement for helium and carbon, while nitrogen and neon are about

TABLE 3
V838 HER ABUNDANCE COMPARISONS

Element	This Work	V96, V97
He ^a	1.4 ± 0.1	1.3
C ^a	7.5 ± 0.7	6.8
N ^a	37.9 ± 5.3	23.7
O ^a	1.9 ± 0.5	0.5
Ne ^a	52.5 ± 2.3	40
Mg ^a	1.4 ± 0.8	...
Al ^a	29 ± 21	...
Si ^a	7.2 ± 2.1	...
S ^a	32.8 ± 3.1	9.5
Fe ^a	1.5 ± 0.4	...

^a By number relative to solar where all abundances taken from Asplund et al. (2005), except for H and Ne, which are from Grevesse & Noels (1993).

40% and 25% lower than in this study. Both oxygen and sulfur in this analysis are about 4 times higher in than Vanlandingham et al. (1996, 1997), but the ratio of the two elements is the same and confirms the large sulfur abundance previously found. With only one date to model, Vanlandingham et al. (1996, 1997) did not derive a magnesium, silicon, or iron abundance. The magnesium and aluminum abundances from our study are each based on only one line from the first two dates, and thus are not as well determined as the other abundances. Magnesium is (probably) not significantly enhanced, while aluminum most likely has a slight enhancement. The iron abundance is consistent with a solar value and probably reflects the initial metallicity of the accreted material, since iron is not expected to be affected by mixing, nor is it created by nucleosynthesis during the thermonuclear runaway (TNR). However, since hydrogen is depleted by the outburst, the H/Fe ratio is expected to decrease.

The distance to V838 Her can be estimated using the predicted luminosities and reddening-corrected fluxes. The distance required to match the observed, corrected flux with the models was calculated for each date and gives a mean distance of 15 kpc. The distance derived using the maximum-magnitude versus rate-of-decline (MMRD) relationship of della Valle & Livio (1995) using $t_2 = 2$ days is 2.7 ± 0.6 kpc. The MMRD distance is consistent with estimates by Starrfield et al. (1992) and Vanlandingham et al. (1996), which show that 3 kpc is a robust value. The discrepancy implies that the covering factors in the multicomponent model are too large. Using the MMRD distance, the two-component models must on average only intercept 7% of emitted luminosity. This result is consistent with a $\sim 5\%$ covering factor from dust reradiation (Woodward et al. 1992), since the dust presumably arises in the densest clumps, where it can be shielded from the harsh radiation of the WD. The remaining $\sim 93\%$ of the model volume is presumably even hotter and more diffuse gas. To test this assumption the D28 model was reanalyzed with the best-fit two-component models, each covering 5%, plus a third component covering the remainder. The third component was set to a low hydrogen density so as to not contribute to the H β luminosity or significantly alter the fit to the line ratios. All parameters were kept the same as before except for varying the third component's initial hydrogen density. The best fit was a density of 1.3×10^7 cm⁻³. The reduced χ^2 only increased to 2.6 in the three-component model.

Dropping the two-component covering factor by more than a factor of 10 also decreased the ejected mass estimate. The corrected ejected mass is $(7.3 \pm 1.9) \times 10^{-6} M_{\odot}$ for a distance of 2.7 kpc. The uncertainty in the distance adds an additional 50% uncertainty to the mass estimate.

This mass is broadly consistent with the optically thick evolution of the early UV spectra. The “Fe curtain” lifts when the column density falls to 10^{24} cm⁻². Assuming a covering factor of 4π sr, a 50% shell thickness, an ejection velocity of 5000 km s⁻¹, and a mean molecular weight of 1.2, the ejected mass is $\sim 10^{-6} M_{\odot}$.

4.2. The V4160 Sgr Model Fits to the D35, D45, and D72 Data

The inner and outer radii of V4160 Sgr were constrained in each model by assuming a minimum and maximum expansion velocity of 4000 and 6000 km s⁻¹, respectively, multiplied by the number of days after outburst. These expansion velocities are consistent with the larger velocities measured for V4160 Sgr. The best two-component model parameters are given in Table 4. The reduced χ^2 for the D35 and D72 models was 1.1 and 1.3. Unfortunately, the D45 model had more free parameters than lines, and thus in a χ^2 sense there can be no best-fit model. However, it is included to show that the abundance solution derived from the other two dates is consistent with this date. Predicted line ratios and χ^2 values are provided in Table 1 for each model. As with V838 Her, the fits are again very good with the largest χ^2 values in the D35 model caused by the fits to some of the weaker neon lines. The problem is that the model does not predict enough [Ne v] (1575 Å), [Ne iv] (1602 Å), and [Ne iv] (4720 Å) flux in the UV while the strong [Ne v] and [Ne iii] in the optical are well fit. The weak neon line discrepancy contributes about 40% to the total χ^2 on D35. The problem disappears on the later dates, when there are fewer lines to constrain the fits and shows how fewer constraints can lead to different results.

The ratio of the clump to diffuse hydrogen density was 10 for the D35 model. The best fits to the other two dates had similar ratios, 9 and 8, but the agreement is driven primarily by the results from the D35 model, which had both UV and optical spectra. This ratio is significantly higher than that found for V838 Her and V1974 Cyg but is consistent with V382 Vel (Shore et al. 2003). The reason for the difference is found in the [Ne v] (3346, 3426 Å) to [Ne iii] (3869, 3968 Å) ratio. For V4160 Sgr it was large, 7.5, on D35. The ratio eventually declined to 3.6 on day 72. In contrast, the same neon ratio was never above 3 on the four V838 Her dates and between 5 and 7 on the three dates modeled in V1974 Cyg. To produce the observed neon ratio the model required an extremely low density diffuse component that was more readily ionized to provide a greater [Ne v] contribution. The physical implication is that V4160 Sgr had a much stronger density gradient in its ejecta than V838 Her or V1974 Cyg. The clump to diffuse covering factor ratio for the first two dates was ≤ 1 , indicating that V4160 Sgr's ejecta volume was dominated only slightly by the diffuse gas. The extreme density gradient implies, however, that the majority of the ejected mass was again in the clumps.

V4160 Sgr showed a luminosity decline similar to V838 Her. After 70 days the model luminosity decreased by a factor of 10, implying that V4160 Sgr also experienced a very rapid end to nuclear burning.

The V4160 Sgr abundance solution confirms what was initially suspected based on the comparison between V4160 Sgr and V838 Her in Figure 2. V838 Her showed stronger carbon and sulfur lines, and the analysis shows that it also had greater enhancement in these elements relative to V4160 Sgr. Likewise, V4160 Sgr had stronger nitrogen and oxygen lines, which is reflected in its higher abundances of these elements. The differences in the oxygen and sulfur imply that V838 Her reached a higher maximum TNR temperature (Starrfield et al. 2001; José et al. 2001).

The same technique used to determine the true two-component covering factor for V838 Her is used for V4160 Sgr, but only the

TABLE 4
V4160 SGR BEST-FIT CLOUDY MODEL PARAMETERS

Parameter	September 2 (D35)	September 12 (D45)	October 9 (D72)	Final Abundances
$T_{\text{BB}} (\times 10^5 \text{ K})^{\text{a}}$	3.2	3.2	2.5	...
Source luminosity ($\times 10^{37} \text{ ergs s}^{-1}$) ^a	10	10	1.0	...
Diffuse hydrogen density ($\times 10^7 \text{ cm}^{-3}$) ^a	1.6	0.5	0.25	...
Clump hydrogen density ($\times 10^7 \text{ cm}^{-3}$) ^a	16	4.5	2.0	...
Inner radius ($\times 10^{15} \text{ cm}$) ^b	1.29	1.62	2.40	...
Outer radius ($\times 10^{15} \text{ cm}$) ^b	1.91	2.45	3.63	...
Clump to diffuse covering factor ratio ^a	40/60	30/70	90/10	...
He/He _⊙ ^{a,c}	1.6 (4)	1.6 (1)	2.1 (3)	1.8 ± 0.1
C/C _⊙ ^{a,c}	4.6 (2)	4.8 (3)	4.0 (0)	4.7 ± 0.1
N/N _⊙ ^{a,c}	155 (5)	155 (3)	124 (3)	147 ± 8
O/O _⊙ ^{a,c}	16.2 (7)	21.9 (2)	18.7 (6)	18 ± 1
Ne/Ne _⊙ ^{a,c}	50 (7)	72 (3)	63 (5)	59 ± 2.3
Mg/Mg _⊙ ^{a,c}	1.1 (0)	12.3 (1)	1.1 (0)	≈10
Si/Si _⊙ ^{a,c}	11 (2)	12.3 (2)	4.4 (0)	11.7 ± 0.5
Fe/Fe _⊙ ^{a,c}	1.1 (2)	1.1 (0)	2.3 (1)	1.5 ± 0.5
Ejected mass ($\times 10^{-5} M_{\odot}$)	13	6.4	5.2	...
Lines used	24	12	15	...
dof ^d	12	0	5	...
Total χ^2	13.41	8.25	6.48	...

^a Free parameter in the optimization. All models had a hydrogen power laws of -3 , filling factors of 0.2 , and filling factor laws of 0 .

^b Calculated assuming an inner and outer expansion velocity of 4000 and 6000 km s^{-1} , respectively. Not a free parameter in the models.

^c Where $\log(\text{solar number abundances relative to hydrogen})$ He: -1.0 , C: -3.61 , N: -4.22 , O: -3.34 , Ne: -3.93 , Mg: -4.47 , Al: -5.63 , Si: -4.49 , S: -4.86 , and Fe: -4.55 (where all abundances are taken from Asplund et al. [2005] except for H and Ne, which are from Grevesse & Noels [1993]). The number in the parentheses indicates the number of Cloudy lines used in the analysis.

^d Equal to the number of observed lines used in the analysis minus the number of free parameters in the model.

D35 model is used since it contained the most lines. Its flux and luminosity are $8.4 \times 10^{-12} \text{ ergs cm}^{-2} \text{ s}^{-1}$ and $1.6 \times 10^{35} \text{ ergs s}^{-1}$, respectively. The MMRD distance for V4160 Sgr is $6.7 \pm 1.5 \text{ kpc}$. At this distance the two-component model requires a covering factor of 28% to fit the data. The final ejected mass for V4160 Sgr is therefore $3.6 \times 10^{-5} M_{\odot}$. This is about a factor of 4 larger than that determined for V838 Her. The larger ejected mass and lack of sulfur in the ejecta implies that the V4160 Sgr outburst occurred on a lower mass WD than in V838 Her.

4.3. Accuracy of Abundance Estimates of Spatially Unresolved Nova Ejecta

The ejecta of both V838 Her and V4160 Sgr were clumpy, even by classical nova standards. The emission line profiles evolved considerably during the outburst, generally from an asymmetric profile (strong blue peak in V838 Her but a strong red peak in V4160 Sgr; see Fig. 3) toward a nearly double peak structure. Given the linear velocity law characteristic of these ejecta, the symmetric profiles are consistent with an axisymmetric (ringlike or annulus) mass distribution, with the other peaks representing individual knots (or agglomerations of unresolved knots as suggested by spatially resolved imaging with *HST* of, for example, HR Del 1967; see Harman & O'Brien 2003). In V838 Her and V4160 Sgr the brightest knots also had the highest expansion velocity, and thus faded faster than the slower moving inner parts of the shell since the emissivity varies as v^{-3} . The results were rapid and dramatic changes in the line profiles of both novae (see Fig. 3). For V838 Her, an important feature is the disappearance of the peaks in the last spectra, indicating that the density in these knots was high enough to continue the recombination even after the rate was globally dominated by the expansion (see Vanlandingham et al. 2005).

With their relatively simple velocity structure, the interpretation of line profile changes in nova ejecta is simpler than usually

possible for stellar winds and jets. Since the radial velocity of the peaks remains invariant even if their relative intensities change, in theory one can assess the physical conditions in the individual knots in much the same way you would approach an interstellar line profile, comparing portions of the ejecta at the same projected velocity among different emission lines of different species (e.g., as done for V1974 Cyg in the integrated and spatially resolved ultraviolet spectra; see Shore et al. 1997). The parts of the profile change differentially because of different densities, and hence different recombination rates. This is particularly evident in the post-freeze-out period (Shore et al. 1996). In practice, however, it can be difficult to disentangle the line contributions of all but the brightest knots. The problem would be alleviated for resolved nova shells, where one could obtain spectral information for individual clumps. This analysis, and the others presented in § 5, uses the information contained within the entire line profile, and thus the model results represent an average of the ensemble clumps. The natural result is an intrinsic scatter in the abundance solutions of unresolved nova when their lines are analyzed in this manner. To estimate the amount of scatter integrating over a line introduces into the analysis of each emission line, we oversimplified each line profile in the V838 Her D60 data set by assuming emission from just two clumps moving in opposite directions. Thus, the line emission was split down the middle into its “blue” and “red” components creating two new line lists for this date. The general effect of these new lines was that the strong neon and the Balmer lines now had “blue” emission lines about 20% stronger than the “red” lines. For both new line lists, Cloudy models were calculated only allowing the electron density and effective temperature to vary. The resulting best-fit “red” model was hotter and denser than the “blue” model, indicating that the ejecta may not be in global ionization equilibrium. Although these parameter differences were small ($\sim 10\%$), they translate into a similar spread in the derived abundance. Monte Carlo techniques (e.g., Ercolano

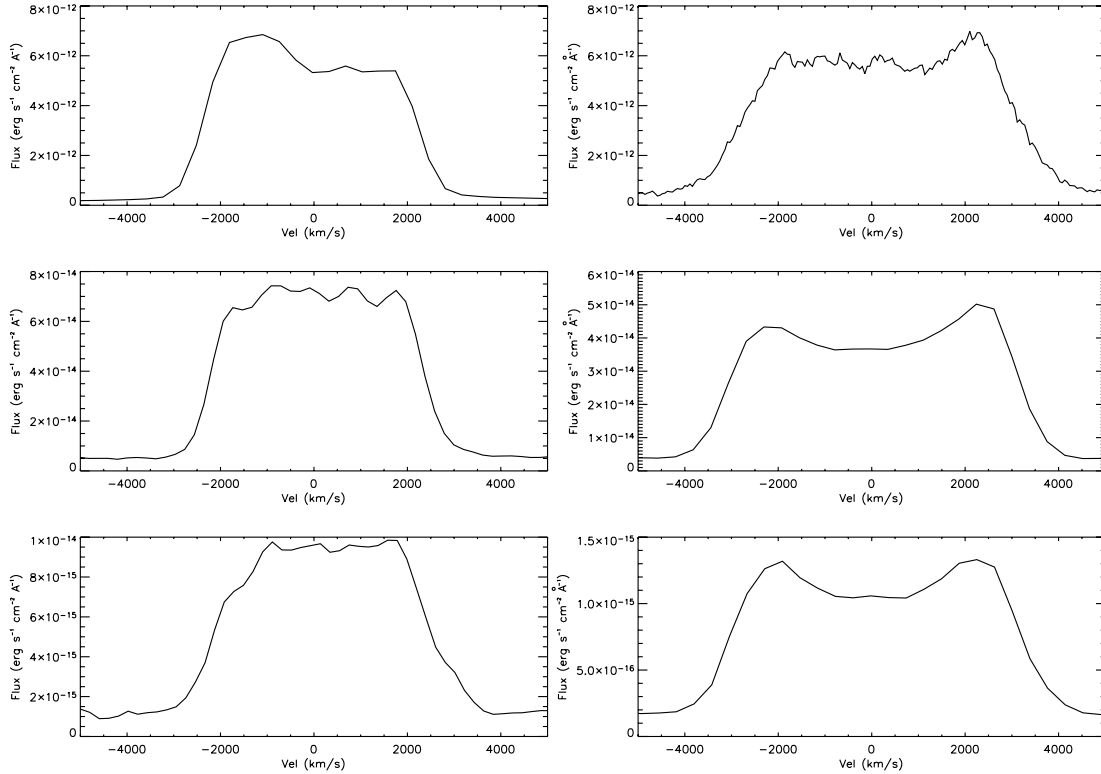


FIG. 3.—Evolution of H α in V838 Her (*left*) and V4160 Sgr (*right*) in velocity space. The V838 Her data from the top down is from 1991 April 3, 1991 May 23, and 1991 August 20. Likewise, the V4160 Sgr data is from 1991 August 1, 1991 September 2, and 1991 October 10.

et al. 2003) may be necessary to correctly model the complex interplay of the knot structure embedded in the diffuse gas, since most current photoionization codes treat the filling factor in an approximate way and only in one dimension. However, by modeling multiwavelength spectra that include lines over a large range of ionization states obtained over many different dates during the

evolution, the uncertainty in the elemental abundance can be significantly reduced.

5. TRENDS IN THE ONeMg NOVA SEQUENCE

Table 5 summarizes the results for all ONeMg novae recently analyzed with the *Cloudy* techniques described in this paper. With

TABLE 5
OBSERVED PROPERTIES AND ESTIMATED PARAMETERS OF FIVE RECENTLY MODELED ONeMg NOVAE

Parameter	QU Vul	V1974 Cyg	V382 Vel	V4160 Sgr	V838 Her
t_2^{opt} (days).....	25	17	4	2	2
t_2^{UVa} (days).....	137 ± 27	71 ± 9	10 ± 1
Dust formation.....	Little	None	None	None?	Little
Turnoff time (days).....	1540	550	230 ± 30	...	<365
M_{eject} ($10^{-5} M_{\odot}$).....	>35	19	18–50	~ 3.6	0.73 ± 0.19
He/H ^b	1.2 ± 0.1	1.2 ± 0.2	1 ^c	1.8 ± 0.1	1.4 ± 0.1
C/H ^b	$0.3_{-0.2}^{+0.1}$	1.0 ± 0.3	0.9	4.7 ± 0.1	7.5 ± 0.7
N/H ^b	18.9 ± 0.7	70 ± 17	26	147 ± 8	37.9 ± 5.3
O/H ^b	3.9 ± 0.1	21 ± 11	5.5	18 ± 1	1.9 ± 0.5
Ne/H ^b	21.7 ± 1.7	42 ± 17	17	59 ± 2.3	52.5 ± 2.3
Mg/H ^b	10.7 ± 0.5	5.2 ± 3.4	2.9	≈ 10	1.4 ± 0.8
Al/H ^b	77.2 ± 8.4	>1.0	26.4	...	29 ± 21
Si/H ^b	2.3 ± 0.1	...	0.5	11.7 ± 0.5	7.2 ± 2.1
S/H ^b	32.8 ± 3.1
Ar/H ^b	0.28 ± 0.02
Fe/H ^b	0.61 ± 0.03	5.8 ± 4.6	...	1.5 ± 0.5	1.5 ± 0.4

NOTE.—Abundance and mass data for QU Vul, V1974 Cyg, V382 Vel, V4160 Sgr, and V838 Her from Schwarz (2002), Vanlandingham et al. (2005), Shore et al. (2003), and Schwarz et al. (this paper), respectively.

^a From Vanlandingham et al. (2001).

^b Where log(solar number abundances relative to hydrogen) He:–1.0, C: –3.61, N: –4.22, O: –3.34, Ne: –3.93, Mg: –4.47, Al: –5.63, Si: –4.49, S: –4.86, Ar: –5.40, and Fe: –4.55 (where all abundances taken from Asplund et al. [2005] except for H, Ne, and Ar, which are from Grevesse & Noels [1993]).

^c The abundances assumed H/He = 1, since no hydrogen lines were available in the UV spectrum used in the abundance determination. If H/He > 1 then the other metals are similarly increased.

TABLE 6
MASS FRACTION COMPARISON OF FIVE RECENTLY MODELED ONeMg NOVAE

Element ^a	QU Vul	V1974 Cyg	V382 Vel	V4160 Sgr	V838 Her	Solar
H.....	6.27E-01	5.52E-01	6.61E-01	4.65E-01	5.62E-01	7.02E-01
He.....	3.01E-01	2.65E-01	2.64E-01	3.34E-01	3.14E-01	2.80E-01
C.....	5.34E-04	1.64E-03	1.69E-03	6.44E-03	1.24E-02	2.99E-03
N.....	9.83E-03	3.24E-02	1.46E-02	5.77E-02	1.79E-02	9.17E-04
O.....	1.85E-02	8.51E-02	2.66E-02	6.06E-02	7.99E-03	8.31E-03
Ne.....	3.21E-02	5.47E-02	2.65E-02	6.47E-02	6.96E-02	1.65E-03
Mg.....	5.79E-03	2.34E-03	1.58E-03	4.29E-03	6.74E-04	6.48E-04
Al.....	2.66E-03	>4.39E-05	1.10E-03	...	1.02E-03	5.58E-05
Si.....	1.24E-03	5.50E-04	3.29E-04	4.90E-03	3.52E-03	6.99E-04
S.....	8.14E-03	3.64E-04
Ar.....	2.79E-05	1.11E-04
Fe.....	6.01E-04	4.99E-03	...	8.41E-04	1.42E-03	1.27E-03
Z.....	7.17E-02	1.82E-01	7.42E-02	1.99E-01	1.22E-01	1.70E-02
CNO.....	2.9E-02	1.19E-01	4.3E-02	1.25E-01	3.8E-02	1.2E-02
O/N.....	1.9E-00	2.6E-00	1.8E-00	1.0E-00	4.0E-01	9.1E-00
O/C.....	3.46E+01	5.19E+01	1.57E+01	9.4E-00	6.4E-01	2.7E-00

NOTE.—Where the $H + He + Z = 1$.

^a Solar values were assumed for elements that did not have reported abundances.

the inclusion of the novae from this paper, the ONeMg sequence is now well sampled from the relatively slow to extremely fast light curve decay times. If WD mass is the primary driver of the properties of classical novae outburst, such as decay times, then this sample provides an excellent representation of how WD mass affects the energetics of the outburst and the composition of the ejecta.

Some of the correlations have been noted elsewhere, such as the relationship between t_2 and t_2^{UV} , and the inverse relationship between t_2 and turnoff time (Vanlandingham et al. 2001). This paper shows for the first time a correlation between t_2 and the ejected mass for a group of ONeMg novae analyzed with the same techniques. We find that the ejected mass declines by a factor of 50 between QU Vul and V838 Her. This trend is predicted by theory, since the most massive WDs and presumably fastest evolving novae accrete less material before they undergo a thermonuclear runaway (Politano et al. 1995; Jose & Hernanz 1998; Yaron et al. 2005). Their predictions are consistent with our results, although the observations of the amounts ejected are not always consistent with the models, particularly at the low WD mass end. In addition, the amount of mass ejected is also a function of other variables, such as the composition of the accreted envelope (Starrfield et al. 2000; Jose & Hernanz 1998), accretion rate (\dot{M}), and core WD temperature (T_{WD}^{core} ; Yaron et al. 2005). For ex-

ample, a factor of 2 decrease in the $1.25 M_{\odot}$ WD luminosity in the Starrfield et al. (2000) model results in a factor of 7 increase in ejected mass. These other dependencies indicate that the ejected mass alone cannot be used to determine the underlying WD mass.

What about the abundance trends versus WD mass reported in the theoretical ONeMg models of Politano et al. (1995) and Jose & Hernanz (1998)? Are there similar tendencies in t_2 among this group of ONeMg novae? Table 6 gives the abundances by mass fraction for each nova in this sample. Perhaps the most striking trend from this analysis is a clear increase in the carbon abundance with speed class. This increase cannot be due to dust formation effects, since both QU Vul and V838 Her (the two extremes of the speed class range) are believed to have formed small amounts of dust. The same propensity, albeit a much smaller gradient, is seen in the Politano et al. (1995) but not in the Jose & Hernanz (1998) hydrodynamical models; see Table 7. Another obvious observation of the 5 nova sample is that the only nova with an observed sulfur abundance above solar is V838 Her, which also has the lowest oxygen abundance. Both hydrodynamic models predict drastically less oxygen and significant sulfur as the WD mass increases. The increasing S/O ratio, as shown in Table 7, is a reflection of higher temperatures during nuclear burning on a massive WD. The results of this work imply that the creation of sulfur

TABLE 7
PREDICTED ABUNDANCES OF LITERATURE MODELS

M_{WD} (M_{\odot})	POLITANO ET AL. (1995) ^a						JOSÉ ET AL. (2001) ^b					
	C (%)	S/O	CNO (%)	Ne (%)	O/N	O/C	C (%)	S/O	CNO (%)	Ne (%)	O/N	O/C
1.0.....	0.6	9.6E-4	14.7	24.7	5.9	18.7	3.0	1.1E-3	25.9	18	5.8	6.3
1.15.....	5.1	1.4E-3	24.6	18	3.3	2.9
1.25.....	4.3	4.5E-2	13.9	23.1	2.9	1.6	6.0	8.4E-3	24.2	18	1.5	1.8
1.35.....	3.5	3.0	13.3	17.4	0.1	0.3	3.6	9.9E-1	23.5	15	0.2	1.1

NOTES.—José et al. (2001) also provides sequences of different mixing amounts. The sequence in the table was selected to approximate the same initial conditions as in Politano et al. (1995).

^a Where $M = 1.6 \times 10^{-9} M_{\odot} \text{ yr}^{-1}$, $L \sim 9.6 \times 10^{-3} L_{\odot}$, and 50% mixing of WD and accreted material.

^b The $M = 2 \times 10^{-10} M_{\odot} \text{ yr}^{-1}$, $L = 10^{-2} L_{\odot}$, and 50% mixing of WD and accreted material sequence.

at the expense of oxygen occurs in a narrow region of parameter space, since V4160 Sgr showed no sulfur enhancement yet had outburst characteristics similar to V838 Her. Finally, there is no trend in the observed neon abundance with speed class. Politano et al. (1995) and Jose & Hernanz (1998) also show little change in the neon abundance except, the most massive models, where the neon mass declines 20%–30%. The theoretical models also predict 3–8 times more neon than in the nova sample.

There are two significant trends in the theoretical models that are not seen in the observed abundances. First, the hydrodynamical models of Politano et al. (1995) and Jose & Hernanz (1998) show an increase in the nitrogen abundance with increasing WD mass. The increases in carbon and nitrogen are offset by the decrease in oxygen, leaving the total CNO abundance of the theoretical models constant to within 10%; see Table 7. A similar nitrogen trend is not observed in the ONeMg sample, and as a consequence the total CNO abundance varies by a factor of 4. This implies differences in the initial CNO abundances, since the CNO cycle neither creates nor destroys CNO. Only V838 Her had depleted CNO. Second, both theoretical models predict significant enhancements of phosphorus, chlorine, and argon in the massive WD models. Emission from these elements is generally not observed, and when it is (e.g., argon in QU Vul) the abundances are subsolar. How can a nova such as V838 Her produce significant silicon and sulfur but none of the other elements in the Si-Ca range? V838 Her is unique in some way.

In general, the observed ejected mass and abundance fractions of the five ONeMg novae mimic many of the gross properties seen in the theoretical hydrodynamic models. However, attempts to fit the individual results to any of the models gives less than satisfying results. While it is possible to find initial conditions that fit the observed range of ejected masses, other predicted outburst characteristics are wrong. The models of Yaron et al. (2005) cover a large span of input parameter space, and thus it is possible to find models that fit the ejected mass and Y_{ej} and Z_{ej} values of these novae. For example, the best fit to QU Vul and V838 Her are the (0.65, 10, -9) and (1.25, 30 or 50, -9) models, respectively, where (M_{WD} , T_{WD}^{core} , M) define the Yaron et al. (2005) model parameters. The best-fit QU Vul model matches the observed ejection velocities, luminosity, and outburst timescales. However, in the best-fit V838 Her model the model ejection velocities are 5 times lower than observed, and the model outburst amplitude of ~ 11.5 gives a quiescent magnitude that is about 4 mag too bright. Using Politano et al. (1995) and Jose & Hernanz (1998) 1.25 M_{\odot} models for V838 Her also does not produce the observed mass fractions, particularly sulfur.

This sample of ONeMg novae, analyzed with the same techniques, is a valuable resource for the modeling community. The diversity in these novae spans not only their observed characteristics (decline time, expansion velocities, etc.), but also their derived ejected abundances and masses. Continued exploration of the theoretical input parameter space, particularly at low accretion rates and WD temperatures, may help alleviate some of the noted discrepancies. Likewise, observationally we need to determine whether these low values are typical of classical novae.

6. CONCLUSIONS

In this paper we analyzed two ONeMg novae, V838 Her and V4160 Sgr, using Cloudy in a mode designed to include the effects of density inhomogeneities in the ejected gas (Vanlandingham et al. 2005; Shore et al. 2003). Our new results for V838 Her build on the previous work of Vanlandingham et al. (1996, 1997) by including more emission lines over more dates. V838 Her and

V4160 Sgr are two of the fastest novae on record and, in addition, are ONeMg novae. Their intrinsic, early spectral development and light curve evolution are nearly identical. The differences observed in the line emission is reflected in the abundance solutions; greater nitrogen and oxygen in V4160 Sgr, while V838 Her has more carbon and sulfur. While many of the conclusions of Vanlandingham et al. (1996, 1997) are verified, including an unusually high S/O ratio and a rapid decline in bolometric luminosity, we find far less mass ejected in the outburst than they reported. The ejected mass of V4160 Sgr, which had the same t_2 time as V838 Her, is estimated to be 4 times greater than in V838 Her. This is consistent with the fact that the expansion velocities were higher in V4160 Sgr and hence the analogous spectral progression with V838 Her.

We compare the amount of mass ejected and ejecta abundances for V838 Her and V4160 Sgr to three other ONeMg novae with less extreme decline rates. Our analyses of these fast novae, in combination with the earlier analyses of the other three novae, allow us to compare novae with a broad range in decline rates. In fact, we have two groups of ONeMg novae: those with extremely rapid decline rates (V382 Vel, V4160 Sgr, and V838 Her) and those with less rapid decline rates (QU Vul and V1974 Cyg) that have all been analyzed with our Cloudy plus optimization technique. The five novae in this sample show a decline in ejected mass with shorter decline times. The decline time is not a sensitive indicator of the ejected mass, as the estimated mass varies over a factor of 30 within $4 \geq t_2 \geq 2$. This range in ejected mass is unexpected if WD mass is the primary controlling variables. However, new theoretical models of Starrfield et al. (2000, 2001) and Yaron et al. (2005) show that the ejected mass is also dependent on variables such as the initial composition of the accreted shell, the WD temperature, and the accretion rate. Whether the low initial WD luminosities ($\sim 10^{-3} L_{\odot}$) and mass accretion rates ($\leq 10^{-10} M_{\odot} \text{ yr}^{-1}$) required by the models is typical for classical nova remains to be seen.

The abundances of this nova sample also confirm many of the trends seen in the theoretical models, including increasing carbon and sulfur with decreasing t_2 and increasing WD mass. In theory, ratios of different elements could be used as a proxy for WD mass, since the abundances of many are dependent on the temperatures achieved during the TNR, which is sensitive to WD mass. For example, Politano et al. (1995) predict O/N < 1 as an indication of an outburst on a massive WD. In our sequence the O/N ratio does decline from 1.9 in QU Vul to 0.4 in V838 Her. Perhaps another WD mass test might be the O/C ratio, since both the model and the observed abundances show increasing carbon and decreasing oxygen with M_{WD} and t_2 , respectively. An O/C ratio ≤ 1 implies a massive WD in the theoretical models (see Table 7), while in the observed ONeMg sample the decline is a factor of 60 between QU Vul and V838 Her.

V838 Her is also unique in this list because its ejecta are enriched in sulfur. The sulfur enrichment, in combination with depleted total CNO, implies that breakout has occurred during the thermonuclear runaway (Starrfield et al. 2007, in preparation). By this we mean that the nuclear burning temperatures were hot enough ($T > 5 \times 10^8$ K) for a significant number of alpha captures to occur on ^{14}O and ^{15}O during the thermonuclear runaway. So far, none of the theoretical simulations have reached such high temperatures. Nevertheless, breakout does not seem to have occurred in either V382 Vel or V4160 Sgr, the other two extremely fast ONeMg novae. Currently, we do not understand why V838 Her is unique, but it could be that the mass of the white dwarf in this system is larger than those in the two other systems, since the

peak temperature in the runaway is a function of white dwarf mass (Politano et al. 1995; Prialnik & Kovetz 1995). It is also possible that differences in the evolutionary history of the white dwarf or in the mass accretion rate onto the white dwarf have contributed to the differences in behavior (Townesley & Bildsten 2004).

We would like to thank M. Wagner and R. Williams for the use of the optical spectra and Gary Ferland for providing his code Cloudy to the public. S. Starrfield acknowledges partial support to ASU from NSF and NASA grants. S. N. S. acknowledges partial support from the University of Pisa and COFIN 2004.

REFERENCES

- Asplund, M., Grevesse, N., & Sauval, A. J. 2005, in ASP Conf. Ser. 336, Cosmic Abundances as Records of Stellar Evolution and Nucleosynthesis, ed. T. G. Barnes III & F. N. Bash (San Francisco: ASP), 25
- Bateson, F. M., Gilmore, A., Camilleri, P., Goltz, W., Williams, P., Bortle, J. E., Jones, A. F., & Seargent, D. A. J. 1991, IAU Circ., 5313, 1
- della Valle, M., & Livio, M. 1995, ApJ, 452, 704
- della Valle, M., & Prins, S. 1991, IAU Circ., 5316, 1
- Dopita, M. A., Sebo, K. M., Gilmore, A. C., Bortle, J. E., & Verdenet, M. 1991, IAU Circ., 5324, 1
- Ercolano, B., Barlow, M. J., Storey, P. J., Liu, X.-W., Rauch, T., & Werner, K. 2003, MNRAS, 344, 1145
- Ferland, G. J., Korista, K. T., Verner, D. A., Ferguson, J. W., Kingdon, J. B., & Verner, E. M. 1998, PASP, 110, 761
- Harman, D. J., & O'Brien, T. J. 2003, MNRAS, 344, 1219
- Harrison, T. E., et al. 1991, IAU Circ., 5223, 1
- Hayward, T. L., et al. 1996, ApJ, 469, 854
- Ingram, D., Garnavich, P., Green, P., & Szkody, P. 1992, PASP, 104, 402
- José, J., Coc, A., & Hernanz, M. 2001, ApJ, 560, 897
- José, J., & Hernanz, M. 1998, ApJ, 494, 680
- Kingsburgh, R. L., English, J., Gilmore, A. C., Bortle, J. E., & Scovill, C. 1991, IAU Circ., 5320, 1
- Lloyd, H. M., O'Brien, T. J., Bode, M. F., Predehl, P., Schmitt, J. H. M. M., Truemper, J., Watson, M. G., & Pounds, K. A. 1992, Nature, 356, 222
- Lynch, D. K., Hackwell, J. A., & Russell, R. W. 1992, ApJ, 398, 632
- Mason, E., della Valle, M., & Bianchini, A. 2002, in AIP Conf. Proc. 637, Classical Nova Explosions, ed. M. Hernanz & J. José (New York: AIP), 214
- Matheson, T., Filippenko, A. V., & Ho, L. C. 1993, ApJ, 418, L29
- O'Brien, T. J., Lloyd, H. M., & Bode, M. F. 1994, MNRAS, 271, 155
- Paresce, F. 1994, A&A, 282, L13
- Paresce, F., Livio, M., Hack, W., & Korista, K. 1995, A&A, 299, 823
- Politano, M., Starrfield, S., Truran, J. W., Weiss, A., & Sparks, W. M. 1995, ApJ, 448, 807
- Prantzos, N., Vangioni-Flam, E., & Casse, M., eds. 1993, Origin and Evolution of the Elements (Cambridge: Cambridge Univ. Press)
- Prialnik, D., & Kovetz, A. 1995, ApJ, 445, 789
- Schlegel, D. J., Finkbeiner, D. P., & Davis, M. 1998, ApJ, 500, 525
- Schwarz, G. J. 2002, ApJ, 577, 940
- Shara, M. M., Zurek, D. R., Williams, R. E., Prialnik, D., Gilmozzi, R., & Moffat, A. F. J. 1997, AJ, 114, 258
- Shore, S. N., Starrfield, S., Ake, T. B., & Hauschildt, P. H. 1997, ApJ, 490, 393
- Shore, S. N., Starrfield, S., & Sonneborn, G. 1996, ApJ, 463, L21
- Shore, S. N., et al. 2003, AJ, 125, 1507
- Starrfield, S., Iliadis, C., Truran, J. W., Wiescher, M., & Sparks, W. M. 2001, Nucl. Phys. A, 688, 110
- Starrfield, S., Shore, S. N., Sparks, W. M., Sonneborn, G., Truran, J. W., & Politano, M. 1992, ApJ, 391, L71
- Starrfield, S., Sparks, W. M., Truran, J. W., & Wiescher, M. C. 2000, ApJS, 127, 485
- Starrfield, S., Truran, J. W., Sparks, W. M., & Krautter, J. 1991, Extreme Ultraviolet Astronomy (New York: Pergamon Press)
- Szkody, P., & Hoard, D. W. 1994, ApJ, 429, 857
- Townesley, D. M., & Bildsten, L. 2004, ApJ, 600, 390
- Vanlandingham, K. M., Schwarz, G. J., Shore, S. N., & Starrfield, S. 2001, AJ, 121, 1126
- Vanlandingham, K. M., Schwarz, G. J., Shore, S. N., Starrfield, S., & Wagner, R. M. 2005, ApJ, 624, 914
- Vanlandingham, K. M., Starrfield, S., & Shore, S. N. 1997, MNRAS, 290, 87
- Vanlandingham, K. M., Starrfield, S., Wagner, R. M., Shore, S. N., & Sonneborn, G. 1996, MNRAS, 282, 563
- Williams, R. E. 1992, AJ, 104, 725
- Williams, R. E., Phillips, M. M., & Hamuy, M. 1994, ApJS, 90, 297
- Woodward, C. E., Gehrz, R. D., Jones, T. J., & Lawrence, G. F. 1992, ApJ, 384, L41
- Yaron, O., Prialnik, D., Shara, M. M., & Kovetz, A. 2005, ApJ, 623, 398